Uranyl to Uranium(IV) Conversion through Manipulation of Axial and Equatorial Ligands

Uranyl to Uranium(IV) Conversion through Manipulation of Axial and Equatorial Ligands

Nicola L. Bell, Brian Shaw, Polly L. Arnold*, Jason B. Love*

EaStCHEM School of Chemistry, The University of Edinburgh, The King's Buildings, Edinburgh, EH9 3FJ, UK

Supporting Information Placeholder

ABSTRACT: The controlled manipulation of the axial oxo and equatorial halide ligands in the uranyl dipyrrin complex, $UO_2Cl(L)$ allows the uranyl reduction potential to be shifted by 1.53 V into the range accessible to naturally occurring reductants that are present during uranium remediation and storage processes. Abstraction of the equatorial halide ligand to form the uranyl cation causes a 780 mV positive shift in the U^V/U^{IV} reduction potential. Borane-functionalization of the axial oxo groups causes the spontaneous homolysis of the equatorial U-Cl bond and a further 750 mV shift of this potential. The combined effect of chloride loss and borane coordination to the oxo groups allows reduction of U^{VI} to U^{IV} by H_2 or other very mild reductants such as Cp^*_2Fe. The reduction with H_2 is accompanied by a B-C bond cleavage process in the oxo-coordinated borane.

Introduction

Over the last decade significant progress has been made in understanding the reduction and oxo-functionalization of the uranyl dication, UO_2^{2+}, in a non-aqueous environment.[1-5] This is important as reduction processes occur within the anaerobic and bacterial environments found in nuclear waste storage and are an important part of protection of the environment by transforming the mobile uranyl(VI) dication to immobile uranium(IV) phases.[6,7] As such, early observations that singly reduced UO_2^+ compounds are isolable,[8,9] and that new oxo-group reactions such as reductive silylation can occur,[10] have led to the extensive exploration of reductive functionalization reactions of uranyl by s-,[11] p-,[12,13] d-,[14] and f-block elements.[15,16] A key factor in accessing reduction to U^V has been shown experimentally and by DFT calculations to be the coordination of the relatively inert -yl oxo groups to electropositive Lewis acids.[11,17,18] This interaction has a strong influence on the U=O bonding and results in the $U^{VI/V}$ redox couple shifting to more positive potentials.[19] Applying these insights has allowed easier reduction to U^{IV}, a process intrinsic to uranium remediation. For example, reductive silylation of UO_2^+ complexes is facilitated by oxo-group functionalization by tris(pentafluorophenyl)borane, $B(C_6F_5)_3$, that shifts the U^V/U^{IV} couple by over 700 mV.[20,21] More recently, the reduction of U^{VI} to U^{IV} with a mild Ti^{III} reductant was promoted by prior O-Ti dative bond formation.[22]

It is also clear that the nature of the equatorial ligand can affect the uranyl reduction potential; $UO_2(Ar_2nacnac)(acac)$ reduces at −1.82 V,[23] while aqueous UO_2^{2+} reduces at −0.35 V vs Fc/Fc^+.[24] Most non-aqueous uranyl reduction reactions exploit complexes of multidentate ligands (e.g. 2 x acac,[25] salen,[26] and pacman[27]) which satisfy the 2+ charge of the uranyl dication whilst minimizing equatorial ligand exchange and disproportionation. In contrast, uranyl complexes of monoanionic multidentate ligand environments which allow coordination of equatorial X-ligands are less studied.[23,28-30]

We recently reported the uranyl complex $UO_2Cl(L)$ **1** of the tetradentate, *mono*anionic, dipyrrin ligand (L) which contains an equatorial chloride ligand (Scheme 1).[22] This complex undergoes controlled inner- and outer-sphere reduction, some of which occurs through the redox activity of L. In this work, we now investigate the role of the equatorial chloride ligand on tuning the reduction potential of the metal, and its complementarity with oxo-group activation by Lewis acidic borane coordination.

Results and Discussion

Uranyl(VI) complexes

Halide abstraction from **1** by $Na[B\{C_6H_2(3,5\text{-}CF_3)_2\}_4]$ ($NaBAr^F$) yields the ion pair $[UO_2(L)][BAr^F]$ **2** which exhibits a diamagnetic ^1H NMR spectrum. In contrast, the reaction of **1** with AgOTf yields the inner-sphere triflate complex $UO_2(OTf)(L)$ which contains a U-O equatorial bond (See SI).

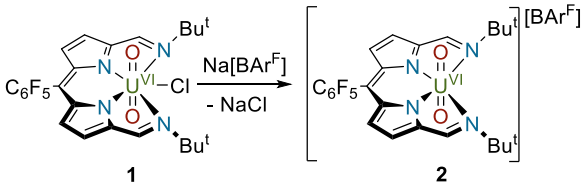

Scheme 1: Halide abstraction from the uranyl dipyrrin complex 1 to form the cationic uranyl complex 2.

The solid-state structure of **2** (Figure 1) displays a vacant equatorial coordination site in the uranium equatorial plane with an N1-U1-N4 angle of 153.8(9)° that is more obtuse than in **1** (149.9(1)°) (Table 1). There is no interaction between the BAr^F anion and the uranium, although the distance between O1 and a fluoroaryl fluorine atom is short (3.556 Å) and within the van der Waals radii. The U=O bond lengths (1.753(2)/1.762(2) Å) are indicative of the U^{VI} oxidation state.

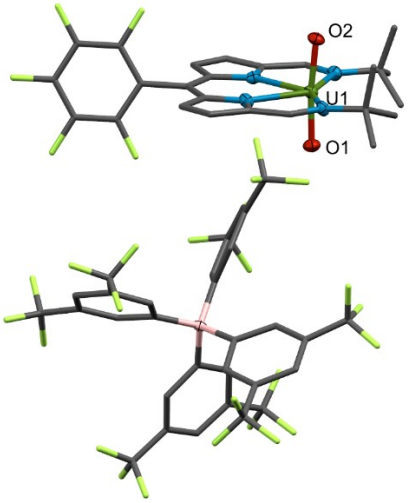

Figure 1. Solid-state structure of **2**. For clarity, all hydrogen atoms and disordered atoms are omitted. Where shown, displacement ellipsoids are drawn at 50% probability. Selected geometric parameters are shown in Table 1.

Uranyl reduction by equatorial ligand substitution

The substitution of the chloride in **1** with 2,6-diisopropylanilide was targeted by reaction with KNHDipp (Dipp = 2,6-*i*Pr$_2$C$_6$H$_3$), but instead yields the paramagnetic, dimeric uranyl(V) complex [UO$_2$(L)]$_2$ **3** (Scheme 2); the ^{1}H NMR spectrum of the reaction mixture shows the presence of the aniline, formed by abstraction of a hydrogen atom from solvent by the aminal radical. The NIR-spectrum of **3** shows a band at 6766 cm^{-1} ($\varepsilon \approx 140$ dm^3 mol^{-1} cm^{-1}) consistent with an *f-f* transition and U^V.

The reduction reaction to form **3** presumably proceeds through the formation of a transient anilide complex UO$_2${NHDipp}(L) which then undergoes U-N bond homolysis. Reduction of uranyl by strong bases such as alkali metal alkyls is well established,[31] and it is notable that the uranyl amide complex UO$_2${N(SiMe$_3$)$_2$}(L), reported previously,[22] slowly degrades by a radical pathway to produce a range of paramagnetic products.

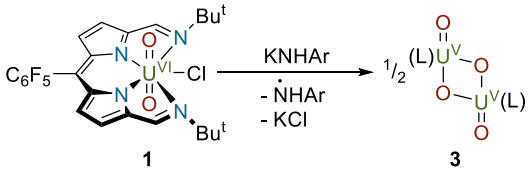

Scheme 2: Reduction of the uranyl(VI) complex 1 to the uranyl(V) dimer 3.

The solid-state structure of **3** (Figure 2) shows a diamond-shaped, oxo-bridging between the two uranyl(V) centers similar to those seen upon reduction of uranyl complexes by lanthanide silylamide reagents.[15] The equatorial U1-O1' bond length (2.377(2) Å) is significantly elongated with respect to the axial bonds U-O1/U-O2 (1.928(2)/1.829(3) Å) with a U···U separation of 3.54 Å. The mass spectra (APPI-MS) of THF or pyridine solutions of **3** contain a molecular ion peak at 1491 *m/z*, consistent with a dimeric structure in solution that is not cleaved by donor solvents.

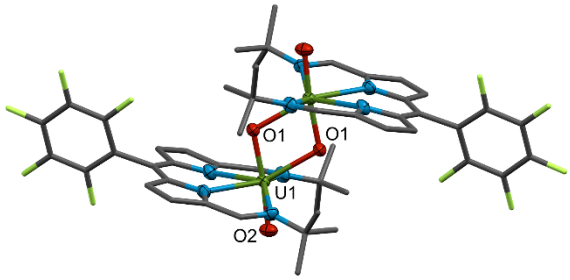

Figure 2: Solid-state structure of **3**. For clarity, all hydrogen atoms are omitted. Where shown, displacement ellipsoids are drawn at 50% probability. Selected geometric parameters are shown in Table 1.

Addition of two equivalents of B(C$_6$F$_5$)$_3$ to dimeric **3** results in a rapid color change from deep purple to bright aquamarine to form the mono(borane) complex UO{OB(C$_6$F$_5$)$_3$}(L) **4** (Scheme 3). The visible color change during this reaction is reflected in a shift of the major UV-vis absorption band from 590 nm in **3** to 617 nm in **4** whilst the higher energy band at 558 nm in **3** decreases in relative intensity and shifts to 572 nm (See SI). The ^{1}H NMR spectrum of **4** exhibits paramagnetically shifted ligand resonances, with the *tert*-butyl resonance appearing at −16.8 ppm compared with −5.97 ppm in **3**. The ^{11}B NMR spectrum shows a single resonance at −149 ppm, while the ^{19}F NMR spectrum shows five resonances for the rigid C$_6$F$_5$ group of L; a very broad resonance at −136 ppm for the *o*-F of the B(C$_6$F$_5$)$_3$ group implies close contact with the U^V center.

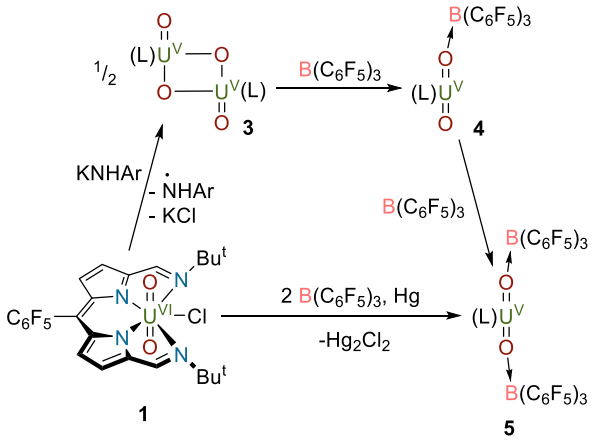

Scheme 3: Lewis acid coordination to uranyl(VI) and uranyl(V) complexes 1 & 3.

The solid-state structure of **4** (Figure 3) shows that cleavage of the cation-cation interaction in **3** by the boron Lewis acid occurs, in contrast to the disproportionation seen upon reaction of [CoCp*$_2$][U^{V}O$_2$(Ar$_2$acnac)$_2$] with B(C$_6$F$_5$)$_3$.[21] The U-O1 bond distance of 1.914(7) Å is comparable to that of other U^V complexes with oxo-coordinated B(C$_6$F$_5$)$_3$,[12] while the U-O2 bond length is shorter at 1.785(7) Å. One of the pentafluorophenyl groups on the coordinated B(C$_6$F$_5$)$_3$ group is twisted in the solid state to yield a relatively short interaction (3.112 Å) between the *ortho*-fluorine atom and the uranium center which may stabilize the monomeric complex.

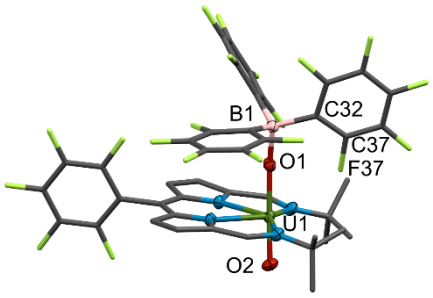

Figure 3: Solid-state structure of **4**. For clarity, all hydrogen atoms and solvents of crystallization are omitted. Where shown, displacement ellipsoids are drawn at 50% probability. Selected geometric parameters are shown in Table 1.

The reaction between **3** and four equivalents of $B(C_6F_5)_3$ yields the borane oxo-functionalized complex $[U\{OB(C_6F_5)_3\}_2(L)$ **5** (Scheme 3). Complex **5** is also directly accessible from **1** through U-Cl bond homolysis. Monitoring the reaction between **1** and two equivalents of $B(C_6F_5)_3$ in C_6D_6 by ^1H NMR spectroscopy shows the formation of an *ca.* 10:1 mixture of **1** and **5** (Scheme 1). The ^{19}F NMR spectrum shows equivalence of the ligand fluorine nuclei as a result of two-fold symmetry, while the ^{11}B NMR spectrum shows one resonance at +110 ppm. The ratio of **1** and **5** neither changes at room temperature over 24 h nor upon heating to 80°C. Increasing the excess of $B(C_6F_5)_3$ to 4 and 8 eq. increases the proportion of **5** in the mixture, forming a **1**:**5** ratio of 2:1 and 1:1, respectively. These observations show that U^{VI}-Cl reductive bond homolysis is driven by manipulation of U=O oxo group bonding, the converse of more usual reactivity involving sterically induced U-X bond homolysis in the equatorial plane. Heating a mixture of $B(C_6F_5)_3$ and **1** in the presence of a source of H$^\bullet$ (dihydroanthracene, 1,4-cyclohexadiene, toluene) to scavenge Cl$^\bullet$ allows the reaction to progress to completion although a number of side products are evident, likely resulting from the formation of HCl. In order to convert **1** to **5** cleanly, elemental mercury was added to reduce the by-product Cl$^\bullet$ to Cl$^-$ in the form of insoluble Hg_2Cl_2 (E_{red} (Hg^I) = + 0.80; E_{red} (Cl$^\bullet$) = + 1.36 V vs NHE). We note that Hg^0 is insufficiently reducing to react with **1** ($E_{1/2}$ = − 0.97 V vs Fc/Fc^+).

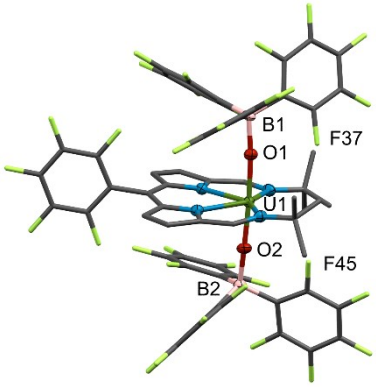

Figure 4: Solid-state structure of **5**. For clarity, all hydrogen atoms and solvents of crystallization are omitted. Where shown, displacement ellipsoids are drawn at 50% probability. Selected geometric parameters are shown in Table 1.

The solid-state structure of **5** shows that both of the uranyl oxo atoms are borane-coordinated and confirms the loss of the equatorial chloride ligand (Figure 4). The U-O bond distances (1.922(3)/1.917(3) Å) are comparable with those of other U^V complexes with $B(C_6F_5)_3$-coordinated oxo groups. As with **2** and **4**, orientation of the *o*-F atom of the $B(C_6F_5)_3$ groups towards the vacant coordination site on the uranium center occurs (3.326/3.526 Å).

Cyclic Voltammetry

The effect of chloride abstraction and oxo-group Lewis acid coordination on the reduction processes of complexes **2-5** was studied by cyclic voltammetry. The processes observed and their assignments are detailed in Table 2 while the reduction waves assigned as the U^V/U^{IV} couple in each voltammogram are shown in Chart 1.

The cyclic voltammogram (CV) of **2** shows an irreversible reduction at −0.64 V vs Fc/Fc^+ and a quasi-reversible reduction wave at −1.24 V (Table 2). The first reduction is assigned as the U^{VI}/U^V couple with its irreversibility indicating the formation of the U^V dimer **3**. The second wave (Chart 1) is assigned as reduction to U^{IV} and represents a +780 mV shift compared with the U^V/U^{IV} reduction seen for **1** (−2.02 V) demonstrating the significant effect of equatorial halide abstraction on the reduction potential of the metal.

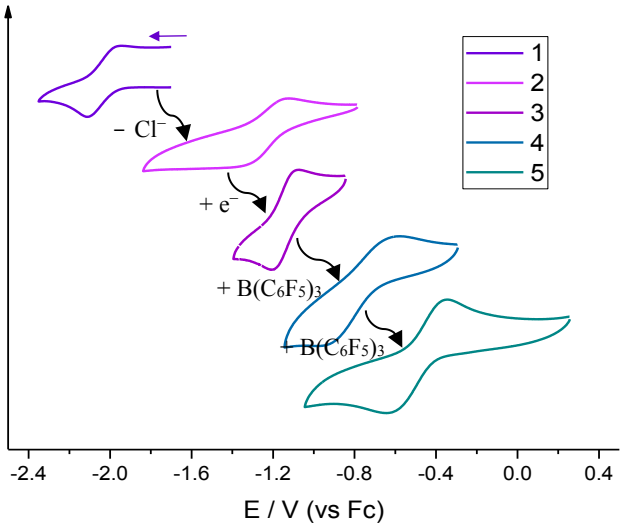

Chart 1: Overlay of the U^V/U^{IV} reduction waves of complexes **1-5** showing a shift of 1.5 V from **1**.

The U^V/U^{IV} reduction process appears at −1.14 V vs. Fc/Fc^+ in the voltammogram of complex **3** (Chart 1). That only one wave is seen for each couple suggests no communication occurs between the two U centers in the dimer and, unlike **1**, no ligand-based reduction is seen. A quasi-reversible oxidation at −0.28 V was also observed and assigned as the U^{VI}/U^V oxidation wave (Table 2). In support of these assignments, the U^{VI} complex **1** is cleanly reformed in ^1H NMR spectrum of the reaction of **3** with CuCl, and the reaction of **3** with Cp^*_2Co results in the formation of a new U^{IV} complex, indicated by paramagnetically shifted ^1H NMR resonances for a single species between 40 and −60 ppm (see SI).

Table 1. Selected U-O and O-B bond distances (Å) and angles (°) for complexes **1**-**7**.

	1	2	3	4	5	6	7
U1-O1 (Å)	1.766(4)	1.753(2)	1.928(2)	1.914(7)	1.922(3)	2.030(5)	2.196(4)
U1-O2 (Å)	1.763(4)	1.762(2)	1.829(3)	1.785(7)	1.917(3)	2.022(5)	1.990(3)
O1-B1 (Å)	-	-	-	1.53(1)	1.578(5)	1.51(1)	1.323(6)
O2-B2 (Å)	-	-	-	-	1.554(5)	1.475(9)	1.490(6)
O-U-O (°)	175.5(2)	173.6(1)	174.5(1)	178.7(3)	176.4(1)	170.6(2)	162.8(1)

Upon coordination of one of the two uranyl oxo atoms to tris(pentafluorophenyl)borane, as in complex **4,** the U^{V}/U^{IV} couple shifts to −0.78 V. Scanning to +1.5 V generates an irreversible oxidation at +1.06 V which presumably corresponds to cleavage of the O-B bond to generate **2** *in situ*. This generates an irreversible reduction wave at −0.41 V which is not present in narrow-window scans and is accordingly attributed to the U^{VI}/U^{V} couple of **2**.

Complex **5**, with both oxo atoms coordinated to $B(C_6F_5)_3$ groups, exhibits a U^{V}/U^{IV} couple at −0.49 V vs Fc/Fc^{+}, representing a shift of +1.53 V versus the same reduction in **1** (−2.02 V). No oxidation wave was observed for complex **5** within the solvent-accessible window.

It is clear from these electrochemical data that the combination of halide removal from the equatorial plane and uranyl oxo-coordination by borane shifts the U^{V}/U^{IV} reduction potential, from −2.02 V in **1** to −0.49 V in **5**, and represents an overall positive shift of 1.53 V; this places the U^{IV} oxidation state within the range of mild reducing agents.

Reduction to U(IV)

The reaction between **5** and decamethylferrocene, Cp^*_2Fe (E_{red} = −0.56 vs Fc/Fc^{+}), yields the U^{IV} anion $[Cp^*_2Fe][U\{OB(C_6F_5)_3\}_2(L)]$ **6** as a deep blue solid (

Scheme 4). The ^1H NMR spectrum of **6** shows paramagnetically shifted resonances between −20 and −52 ppm, indicative of the U^{IV} oxidation state, along with a broad resonance at −30 ppm for $[Cp^*_2Fe]^{+}$. The absorption spectrum of **6** in the near-IR spectrum shows broad bands at 7502 cm^{-1} (ε ≈ 50 dm^3 mol^{-1} cm^{-1}), 9259 cm^{-1} (ε ≈ 160 dm^3 mol^{-1} cm^{-1}) and 9709 cm^{-1} (ε ≈ 200 dm^3 mol^{-1} cm^{-1}).

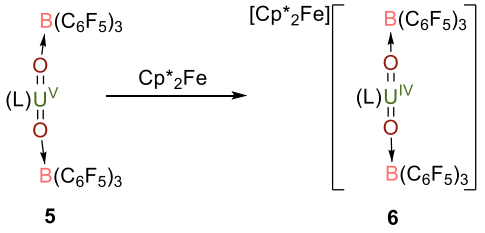

5 6

Scheme 4: Outer-sphere reduction of complex 5 by Cp^*_2Fe yielding the uranium(IV) complex 6.

The solid-state structure of **6** (Figure 5) displays U-O bonds (U1-O1: 2.030(5) Å, U1-O2: 2.022(5) Å) which are elongated by ca. 0.1 Å relative to the uranyl(V) complex **5** (Table 1). The U1···F37/ U1···F45 distances, which were relatively short in **2** and **5**, are significantly longer in **6** (U1···F37: 3.994(5) Å, U1···F45: 3.983(5) Å) and the O-B-C-C torsion angles are larger (O1-B1-C32-C37: 42(1)°; O2-B2-C44-C45: −20(1)°) suggesting minimal interaction between these atoms and the metal center in the U(IV) oxidation state. It is, however, interesting to note that the O-U-O unit remains linear (170.6(2)°).

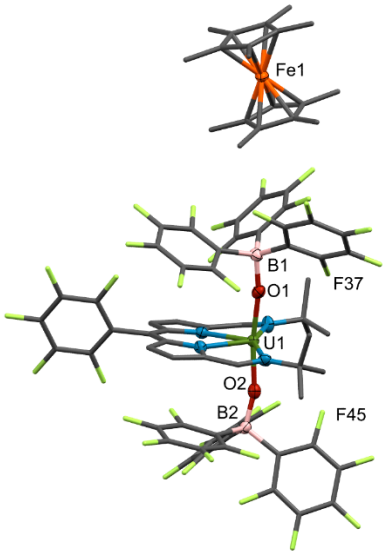

Figure 5: Solid-state structure of **6**. For clarity, all hydrogen atoms and solvents of crystallization are omitted. Where shown, displacement ellipsoids are drawn at 50% probability. Selected geometric parameters are shown in Table 1.

The mildly oxidizing nature of **5** demonstrated by the above experiments contrasts that seen for the majority of uranyl complexes reported to date and led us to investigate dihydrogen as a simple reducing agent of greater relevance to real-world uranyl chemistry; H_2 is formed from radiolysis of water in spent nuclear fuel storage ($E_{1/2}$ (H_2) = −0.54 V vs Fc/Fc^{+}).[32,33] Heating an *o*-difluorobenzene solution of **5** under 1 bar of H_2 yields the deep aquamarine blue U^{IV} complex $U\{OB(C_6F_5)_2\}\{OB(C_6F_5)_3\}(L)$ **7** (Scheme 5). The ^1H NMR spectrum of **7** shows four resonances between −19 and −55 ppm, indicative of U^{IV}, while the ^{11}B NMR spectrum shows two resonances at +150 and −7.70 ppm, suggesting that desymmetrization of the U-O bonds has occurred.

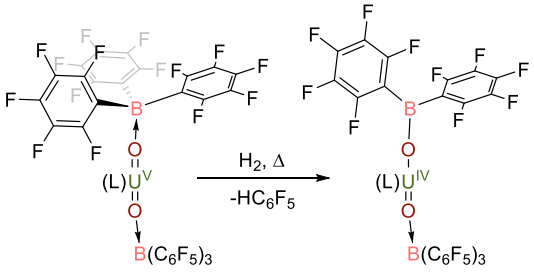

5 7

Scheme 5: Reduction of complex 5 by dihydrogen yielding the U(IV) complex 7.

Table 2. Summary of cyclic voltammetry data for compounds **1**-**5**. Values are from voltammograms recorded at 300 mV s^{-1} in *o*-difluorobenzene and all potentials are referenced against the Fc^{+}/Fc couple.

COMPLEX	PROCESS	E_{PC} / V	E_{PA} / V	ΔE / V	$E_{1/2}$ / V	REVERSIBILITY	RED/OX	ASSIGNMENT
KL[22]	I	–1.29	–	–	–	Irreversible	Reduction	$L^{-}/L^{\bullet-}$
	II	–1.57	–	–	–	Irreversible	Reduction	$L^{\bullet-}/L^{3-}$
1[22]	I	–1.03	–0.89	0.14	–0.96	Quasi-reversible	Reduction	$L^{-}/L^{\bullet-}$
	II	–1.25	–1.10	0.15	–1.18	Quasi-reversible	Reduction	U^{VI}/U^{V}
	III	–2.10	–1.94	0.16	–2.02	Quasi-reversible	Reduction	U^{V} / U^{IV}
2	I	–0.64	-	-	-	Irreversible	Reduction	U^{VI}/U^{V}
	II	–1.37	–1.12	0.25	–1.24	Quasi-reversible	Reduction	U^{V} / U^{IV}
3	I	–0.37	–0.19	0.28	–0.28	Quasi-reversible	Oxidation	U^{VI}/U^{V}
	II	–1.20	–1.07	0.13	–1.14	Quasi-reversible	Reduction	U^{V} / U^{IV}
4	I	+1.06	-	-	-	Irreversible	Oxidation	U^{VI}/U^{V}
	II	-	–0.41	-	-	Irreversible	Reduction	U^{VI}/U^{V}
	III	–0.89	–0.66	0.23	–0.78	Quasi-reversible	Reduction	U^{V} / U^{IV}
5	I	–0.73	–0.26	0.47	–0.49	Quasi-reversible	Reduction	U^{V} / U^{IV}

The solid-state structure of **7** shows that reaction of **5** with H_2 has resulted in the cleavage of one of the borane B-C bonds to yield U-OB(C_6F_5)$_2$ (Figure 6). Reduction of U^{V} to U^{IV} results in an elongation of the U1-O1 bond (2.196(4) Å) relative to that in **5** (1.922(3) Å) while the U1-O2 bond length only increases slightly (1.990(3) Å). Concurrently, O1-B1 bonding is strengthened (1.323(6) Å) relative to O2-B2 (1.490(6) Å) and to the same bonds in **5** (O1-B1: 1.578(5), O2-B2: 1.554(5) Å). The O1-U1-O2 bond angle is decreased (162.8(1)°) relative to that in **6** (170.6(2)°) demonstrating a decrease in oxo-group π-donation. Whilst unexpected, B-C bond cleavage is not unprecedented for oxo-coordinated B(C_6F_5)$_3$. The Sc^{I} complex {BrMg(L)}$_2$ScBr (L = ($R_2NCH_2CH_2NCMe)_2CH$, R = Et) reacts with H_2O:B(C_6F_5)$_3$ to yield (L)Sc{OB(C_6F_5)$_2$} and HC_6F_5,[34] while the related aluminum complex (L)$_2$Al=OB(C_6F_3)$_3$ undergoes aryl migration at elevated temperatures to yield (L)$_2$Al(C_6F_5){OB(C_6F_5)$_2$}.[35]

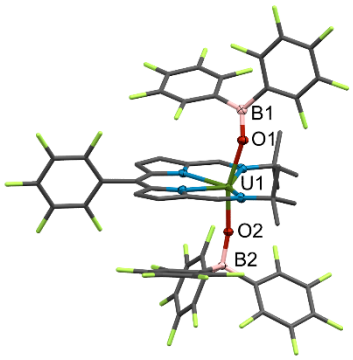

Figure 6: Solid-state structure of **7**. For clarity, all hydrogen atoms, solvents of crystallization, the BAr^{F} anion in **2**, and the Cp*$_2$Fe cation in **6** are omitted. Where shown, displacement ellipsoids are drawn at 50% probability. Selected geometric parameters are shown in Table 1.

Conclusions

The investigations above reveal that by manipulating both the equatorial coordination sphere and the axial oxo-ligand bonding in uranyl complexes it is possible to shift the non-aqueous $U^{VI/V}$ and $U^{V/IV}$ reduction potentials to values in the range accessible to reductants that are present during uranium remediation processes and in nuclear fuel storage. In contrast to aqueous uranyl chemistry, no disproportionation reactions are seen; substitutionally inert uranyl(V) complexes are isolated, allowing the stepwise reduction pathways to be elucidated. Furthermore, the observation of U^{VI} reduction through homolytic equatorial bond cleavage that is promoted by Lewis acid bonding to the uranyl oxo group may have mechanistic implications for environmental uranyl reduction.[6,7]

Experimental section

Synthesis and characterization of complexes 2-7

[UO_2(L)][BAr^{F}], **2**

To a purple solution of **1** (200 mg, 0.256 mmol) in CH_2Cl_2 (10 mL) was added a solution of Na(BAr^{F}_4) (227 mg, 0.256 mmol, 1 eq) in CH_2Cl_2 (10 mL) resulting in the formation of a dark royal blue solution. The reaction mixture was stirred for 16 h before filtration. The filtrate was cooled to –30 °C yielding royal blue crystals, which were isolated by filtration and dried under vacuum for 16 h (220 mg, 53.4%). X-ray quality crystals were grown by slow diffusion of hexane into a concentrated solution of **2** in CH_2Cl_2. ^{1}H NMR (CD_2Cl_2, 500 MHz): δ 9.98 (s, 2H, imine), 7.72 (m, 8H, BAr^{F}_4), 7.55 (s, 4H, BAr^{F}_4), 7.47 (d, 2H, pyrrole), 7.22 (d, 2H, pyrrole), 2.33 (s, 18H, *t*Bu) ppm; ^{13}C NMR (126 MHz, CD_2Cl_2): δ 162.5 (C_q), 159.7 (CH), 147.9 (C_q), 136.67 (C-F), 135.4 (CH), 126.3 (BAr^{F}_4), 125.4 (CH), 124.1 (BAr^{F}_4), 121.9 (BAr^{F}_4), 118.35 – 117.7 (m, BAr^{F}_4), 64.2 (2 x $C(CH_3)_3$), 29.9 (6 x $C(CH_3)_3$) ppm; ^{19}F NMR (471 MHz, CD_2Cl_2) δ −62.9 (s, 24F, CF_3), −138.0 (dd, *J* = 16.2 Hz, 2F), −149.2 (dd, *J* = 21.1 Hz, 1F), −159.6 (m, 2F); Anal. Calcd for $C_{49}H_{36}BF_{13}N_4O_2U$ (M_r = 1608.73 g mol^{-1}): C, 42.55; H, 2.26; N, 3.48; %. Found: C, 42.25; H, 2.30; N, 3.48; %; FTIR (nujol): ν / cm^{-1} 1605 (m, L), 1546 (s, L), 1503 (m, L), 1461 (s, L), 1378 (s, L), 1355 (s, L), 1280 (s, L), 1248 (s, L), 1219 (m, L), 1159 (s, L), 1120 (s, L), 1061 (s, L), 1012 (s, L), 992 (s, L), 952 (s, UO_2 asymmetric stretch), 883 (m, L), 838 (w, L), 813 (w, L), 776 (w, L), 760 (w, L), 713 (m, L), 682 (w, L), 668 (w, L) L = absorptions attributed to the dipyr-

rin ligand.; UV/vis (*o*-$F_2C_6H_4$): λ / nm 393 (ε = 3,150 dm^3 mol^{-1} cm^{-1}), 557 (ε = 12,800 dm^3 mol^{-1} cm^{-1}), 598 (29,800 dm^3 mol^{-1} cm^{-1}).

$[UO_2(L)]_2$, **3**

To a purple toluene solution of **1** (1 g, 1.5 mmol, 1 eq.) was added a colorless toluene suspension of KNHDipp (323 mg, 1.5 mmol, 1 eq.). A golden microcrystalline precipitate formed immediately. The solution was centrifuged, filtered and washed with toluene (3 x 10 mL). The golden precipitate was then extracted into THF (ca. 50 mL) and filtered through Celite with washing (2 x 10 mL). The solvent volume of the purple filtrate was halved and the solution layered with hexane (ca. 1:1 ratio) to yield golden crystals which were filtered and dried to yield **3** as a purple solid (751 mg, 67%). **3** is insoluble in arene solvents but is soluble in donor solvents or halogenated arenes. Dissolution in CH_2Cl_2 results in slow chlorine-atom abstraction to yield **1**. X-ray quality crystals were grown by slow diffusion of hexane into a concentrated solution of **3** in THF. ^{1}H NMR (500 MHz, C_5H_5N): δ −4.23 to −5.19 (br. m, 4H), −5.61 (br. s, 2H), −5.97 (br. s, 18H) ppm; ^{1}H NMR (500 MHz, d_8-THF): δ −5.77 (br. s) ppm; ^{19}F NMR (471 MHz, C_6D_6): δ −145.6, −151.4, −157.0, −164.8, −166.7 ppm; Anal. Calcd for $C_{25}H_{24}F_5N_4O_2U$ (M_r = 1491.02 g mol-1): C, 40.28; H, 3.25; N, 7.52; %. Found: C, 40.06; H, 3.16; N, 7.42 %; APPI-MS (pyridine): 1491.4 m/z; FTIR (Nujol): ν / cm^{-1} 1652 (w, L), 1602 (m, L), 1553 (s, L), 1515 (s, L), 1497 (s, L), 1466 (s, L), 1400 (m, L), 1378 (s, L), 1350 (s, L), 1287 (s, L), 1266 (s, L), 1214 (s, L), 1191 (s, L), 1053 (s, L), 995 (s, L), 951 (m, L), 848 (s, L), 820 (m, L), 783 (s, asym. UO_2 stretch), 759 (s, L), 713 (m, L), 674 (s, U-O_{eq}), 641 (w, L), L = absorptions attributed to the dipyrrin ligand. UV/vis (*o*-$F_2C_6H_4$): λ / nm 393 (ε = 3,150 dm^3 mol^{-1} cm^{-1}), 522 (ε = 9300 dm^3 mol^{-1} cm^{-1}), 559 (ε = 42,400 dm^3 mol^{-1} cm^{-1}), 591 (41,500 dm^3 mol^{-1} cm^{-1}). Near-IR (*o*-$F_2C_6H_4$): 6766 (ε ≈ 140 dm^3 mol^{-1} cm^{-1}).

$UO\{OB(C_6F_5)_3\}(L)$, **4**

To a purple solution of **3** (200 mg, 0.13 mmol, 1 eq.) in toluene (ca. 5 mL) was added a colorless solution of tris(pentafluorophenyl)borane (137.4 mg, 0.27 mmol, 2 eq.) in toluene (ca. 5 mL). The solution immediately turned bright aquamarine blue. The reaction mixture was allowed to stand at room temperature for 16 h, during which orange crystals formed which were filtered and dried to yield **5** as a purple solid (296 mg, 87%). X-ray quality crystals were grown by slow diffusion of hexane into a concentrated solution of **4** in dioxane. ^{1}H NMR (500 MHz, C_6D_6): δ −4.82 (s, 2H), −6.11 (s, 2H), −12.72 (s, 2H), −16.83 (s, 18H) ppm; ^{19}F NMR (471 MHz, C_6D_6): δ −135.8 (br. s, 6F, o-B(C_6F_5)$_3$), −140.8 (d, *J* = 21.9 Hz, 1F), −148.1 (d, *J* = 22.6 Hz, 1F), −153.0 (t, *J* = 22.3 Hz, 1F), −158.0 (d, *J* = 17.9 Hz, 3F, p-B(C_6F_5)$_3$), −161.15 (t, *J* = 20.5 Hz, 1F), −162.98 (d, *J* = 19.1 Hz, 6F, m-B(C_6F_5)$_3$), −164.4 (t, *J* = 22.2 Hz, 1F) ppm; ^{11}B NMR (161 MHz, C_6D_6): δ 149 ppm. Anal. Calcd for $C_{43}H_{24}BF_{20}N_4O_2U$ (M_r = 1257.50 g mol^{-1}): C, 41.07; H, 1.92; N, 4.46; %. Found: C, 41.19; H, 2.03; N, 4.53 %; FTIR (Nujol): ν / cm^{-1} 1646 (w, L), 1602 (w,L), 1544 (m,L), 1518 (m, L), 1467 (s, L), 1377 (m, L), 1251 (m, L), 1217 (m, L), 1185 (m, L), 1089 (m, L), 1075 (w, L), 1061 (m, L), 1007 (s, L), 993 (m, L), 973 (m, L), 954 (m, L), 874 (w, L), 851 (w, L), 837 (m, UO2 asymm. stretch), 814 (m, L), 761 (w, L), 723 (w, L), 673 (w, L) L = absorptions attributed to the dipyrrin ligand; UV/vis (toluene): λ / nm 306 (ε = 29,500 dm^3 mol^{-1} cm^{-1}), 572 (ε = 17, 100 dm^3 mol^{-1} cm^{-1}), 617 (46,700 dm^3 mol^{-1} cm^{-1}); Near-IR (*o*-$F_2C_6H_4$): 6468 (ε ≈ 125 dm^3 mol^{-1} cm^{-1}).

$U\{OB(C_6F_5)_3\}_2(L)$, **5**

To a purple solution of **1** (1 g, 1.50 mmol) in *o*-difluorobenzene (15 mL) was added and excess of elemental mercury prior to the addition of tris(pentafluorophenyl)borane (1.79 g, 3.0 mmol, 2 eq). The solution immediately turned bright aquamarine blue and a colorless precipitate formed. The solution was filtered to remove excess Hg along with the colorless salt (Hg_2Cl_2) and extracted with *o*-difluorobenzene (2 x 10 mL). The solvent was removed from the filtrate yielding **5** as a deep aquamarine blue solid (2.41 g, 91%). Alternatively, **5** can be synthesized by addition of two equivalents of tris(pentafluorophenyl)borane to **3**. X-ray quality crystals were grown by slow diffusion of hexane into a concentrated solution of **5** in a mixture of *o*-difluorobenzene and C_6D_6. ^{1}H NMR (500 MHz, C_6D_6): δ −3.56 (d, *J* = 4.0 Hz, 2H), −3.70 (d, *J* = 4.0 Hz, 2H), −6.76 (s, 2H), −14.82 (s, 18H); ^{19}F NMR (471 MHz, C_6D_6): δ −126.7 (br. s, 12F, o-B(C_6F_5)$_3$), −144.4 (d, *J* = 16.5 Hz, 2F), −150.9 (t, *J* = 22.3 Hz, 1F), −159.2, −163.7 (m, 20F, m-B(C_6F_5)$_3$ (12F) + p-B(C_6F_5)$_3$ (6F)+ ArF (2F)); ^{11}B NMR (161 MHz, C_6D_6): δ 110 ppm; Anal. Calcd for $C_{61}H_{24}B_2F_{35}N_4O_2U$ (M_r = 1769.48 g mol^{-1}): C, 41.41; H, 1.37; N, 3.17; %. Found: C, 41.53; H, 1.46; N, 2.97 %; FTIR (Nujol): ν / cm^{-1} 1711 (w), 1647 (m), 1598 (w), 1547 (m), 1528 (m), 1518 (s), 1500 (m), 1460 (vs), 1377 (s), 1354 (m), 1285 (m), 1251 (m), 1217 (m), 1181 (m), 1098 (m), 1066 (m), 1023 (m), 1014(m), 993 (m), 978 (m), 954 (m), 851 (m), 834 (w), 820 (w), 814 (m), 810 (m), 800 (br., m), 780 (m), 774 (m), 769 (br., m), 762 (m), 753 (br., m), 743 (br., m), 737 (m), 734 (m), 726 (s), 723 (s), 684 (m), 680 (br., w) 673 (m,), 652 (w), 652 (w); UV/vis (toluene): λ / nm 304 (ε = 36,400 dm^3 mol^{-1} cm^{-1}), 397 (ε = 2,800 dm^3 mol^{-1} cm^{-1}), 536 (ε = 3,630 dm^3 mol^{-1} cm^{-1}), 573 (14,320 dm^3 mol^{-1} cm^{-1}), 617 (49,500 dm^3 mol^{-1} cm^{-1}), 650 (ε = 9,250 dm^3 mol^{-1} cm^{-1}); Near-IR (*o*-$F_2C_6H_4$): 6609 (ε ≈ 160 dm^3 mol^{-1} cm^{-1}).

$[Cp^*_2Fe][UO\{OB(C_6F_5)_3\}(L)]$, **6**

To a purple solution of **2** (200 mg, 0.13 mmol, in ca 5mL) in toluene (10 mL) was added a solution of decamethylferrocene (37 mg, 0.13mmol, in ca. 5 mL) in toluene (10 mL). The solution immediately turned deep aquamarine blue and deep blue oil precipitated from solution. The oil was redissolved in *o*-difluorobenzene (3mL) and layering with hexanes resulted in the formation of red crystals upon standing for 16 h at room temperature. The crystals were filtered, washed with hexanes and dried under reduced pressure to yield **6** (201 mg, 85%). X-ray quality crystals were grown by slow diffusion of hexane into a concentrated solution of **6** in *o*-difluorobenzene. ^{1}H NMR (500 MHz, C_6D_6): δ −19.96 (s, 2H), −25.54 (s, 2H), −34.88 (s, 30H), −39.45 (s, 2H), −51.71 (s, 18H) ppm; ^{19}F NMR (471 MHz, C_6H_5Cl): δ −104.8 (br. s, 12F, o-B(C_6F_5)$_3$), −153.8 (s, 2F) −158.9 (s, 6F, p-B(C_6F_5)$_3$), −160.70 (s, 12F), −165.2 (t, 18.5 Hz, 1F), −168.7 (d, J = 18.5 Hz, 2F, m-B(C_6F_5)$_3$); ^{11}B NMR (161 MHz, C_6H_5Cl): δ 412.3 (br. s, 1B), 425.8 (br. s, 1B) ppm; Anal. Calcd for $C_{81}H_{54}B_2F_{35}FeN_4O_2U$ (M_r = 2095.79 g mol^{-1}): C, 46.42; H, 2.60; N, 2.67; %. Found: C, 45.95; H, 2.51; N, 2.51 %; FTIR (Nujol): ν / cm^{-1} 1609 (m,L), 1560 (s,L), 1521 (m, L), 1499 (s, L), 1459 (vs, L), 1407 (m, L), 1377 (m, L), 1277 (vs, L), 1274 (vs, L), 1219 (w, L), 1193 (m, L), 1062 (m, L), 1000 (vs, L), 982 (s, L), 962 (w, L), 948 (m, L), 846 (s, L), 814 (s, L), 771 (w, L), 727 (w, L), 631

(vs, UO_2 asymmetric stretch) L = absorptions attributed to the dipyrrin ligand; UV/vis (toluene): λ / nm 307 (ε = 32,400 dm^3 mol^{-1} cm^{-1}), 573 (17,900 dm^3 mol^{-1} cm^{-1}), 617 (59,300 dm^3 mol^{-1} cm^{-1}); Near-IR (*o*-$F_2C_6H_4$): 6579 (ε ≈ 100 dm^3 mol^{-1} cm^{-1}), 7502 (ε ≈ 150 dm^3 mol^{-1} cm^{-1}); 9259 (ε ≈ 160 dm^3 mol^{-1} cm^{-1}); 9709 (ε ≈ 200 dm^3 mol^{-1} cm^{-1}).

U{OB(C_6F_5)$_2$}{OB(C_6F_5)$_3$}(L), **7**

A Teflon-tapped ampoule containing a deep aquamarine blue solution of **2** (480 mg) in *o*-difluorobenzene (5 mL) was charged with H_2 (1 bar). The solution was stirred with heating for 12 h before the half of the solvent was evaporated under vacuum. The remaining solution was layered with hexane yielding **7** as dark blue needles (284 mg, 66%). X-ray quality crystals were grown by slow diffusion of hexane into a concentrated solution of **7** in 1,1,1-trifluorotoluene. ^{1}H NMR (500 MHz, C_6D_6): δ −19.85 (s, 2H), −25.29 (s, 2H), −36.94 (s, 2H), −50.86 (s, 18H); ^{11}B NMR (161 MHz, C_6D_6): δ 150.3, −7.7 ppm; ^{19}F NMR (376 MHz, C_6D_6/C_6H_5Cl) δ −88.9 (d, 4F, *o*-F), −131.0 (br., 6F, *o*-F), −143.7 (t, *J* = 19.1 Hz, 2F, *p*-F), −150.7 (d, *J* = 19.6 Hz, 4F, *m*-F), -153.8 (d, *J* = 23.3 Hz, 1F, *o*-F), -154.2 (m, 1F, *o*-F), −155.9 - −156.5 (m, 3F, *p*-F), −160.4 (d, *J* = 20.8 Hz, 6F, *m*-F), −162.2 (dt, *J* = 22.6, 11.6 Hz, 1F, *p*-F), −166.0 (m, 1F, *m*-F), −167.2 (t, *J* = 22.6 Hz, 1F, *m*-F); ^{11}B NMR (161 MHz, C_6D_6) δ 450 (br. s, 1B), 425 (s, 1B) ppm; Anal. Calcd for $C_{55}H_{24}B_2F_{30}N_4O_2U$ (M_r = 1602.42 g mol^{-1}): C, 41.23; H, 1.51; N, 3.50; %. Found: C, 41.08; H, 1.39; N, 3.72 %; FTIR (Nujol): ν / cm^{-1} 1647 (m), 1602 (w), 1545 (m), 1516 (m), 1465 (s), 1377 (m), 1308 (w), 1280 (w), 1250 (m), 1217 (w), 1190 (w), 1086 (m), 1063 (m), 1011 (m), 989 (m), 975 (m), 850 (w), 832 (w), 774 (w), 760 (w), 722 (w), 686 (w). UV/vis (toluene): λ / nm 315 (ε = 20,100 dm^3 mol^{-1} cm^{-1}), 578 (15,290 dm^3 mol^{-1} cm^{-1}), 622 (47,450 dm^3 mol^{-1} cm^{-1}); Near-IR (*o*-$F_2C_6H_4$): 6464 (ε ≈ 30 dm^3 mol^{-1} cm^{-1}), 7220 (ε ≈ 40 dm^3 mol^{-1} cm^{-1}); 8562 (ε ≈ 70 dm^3 mol^{-1} cm^{-1}).

ASSOCIATED CONTENT

The Supporting Information is available free of charge via the internet at http://pubs.acs.org. General experimental conditions, NMR, CV, UV-vis-NIR, X-ray crystallographic data (PDF).

AUTHOR INFORMATION

Corresponding Authors

Polly.Arnold@ed.ac.uk; Jason.Love@ed.ac.uk

ORCID

Polly L. Arnold: 0000-0001-6410-5838

Jason B. Love: 0000-0002-2956-258X

Nicola L. Bell: 0000-0002-7497-9667

Notes

The authors declare no competing financial interests.

ACKNOWLEDGMENT

The authors thank the University of Edinburgh and the EPSRC (Grant number EP/M010554/1) for funding. This project has received funding from the European Research Council (ERC) under the European Union's Horizon 2020 research and innovation programme (grant agreement No 740311).

REFERENCES

(1) Liddle, S. T. *Angew. Chem. Int. Ed.* **2015**, *54*, 8604.
(2) Jones, M. B.; Gaunt, A. J. *Chem. Rev.* **2013**, *113*, 1137.
(3) Baker, R. J. *Chem. Eur. J.* **2012**, *18*, 16258.
(4) Fortier, S.; Hayton, T. W. *Coord. Chem. Rev.* **2010**, *254*, 197.
(5) Arnold, P. L.; Love, J. B.; Patel, D. *Coord. Chem. Rev.* **2009**, *253*, 1973.
(6) Cumberland, S. A.; Douglas, G.; Grice, K.; Moreau, J. W. *Earth Sci. Rev.* **2016**, *159*, 160.
(7) Natrajan, L. S.; Swinburne, A. N.; Andrews, M. B.; Randall, S.; Heath, S. L. *Coord. Chem. Rev.* **2014**, *266-267*, 171.
(8) Natrajan, L.; Burdet, F.; Pecaut, J.; Mazzanti, M. *J. Am. Chem. Soc.* **2006**, *128*, 7152.
(9) Berthet, J.-C.; Siffredi, G.; Thuery, P.; Ephritikhine, M. *Chem. Commun.* **2006**, 3184.
(10) Arnold, P. L.; Patel, D.; Wilson, C.; Love, J. B. *Nature* **2008**, *451*, 315.
(11) Arnold, P. L.; Pécharman, A.-F.; Hollis, E.; Yahia, A.; Maron, L.; Parsons, S.; Love, J. B. *Nat. Chem* **2010**, *2*, 1056.
(12) Pedrick, E. A.; Wu, G.; Kaltsoyannis, N.; Hayton, T. W. *Chem. Sci.* **2014**, *5*, 3204.
(13) Jones, G. M.; Arnold, P. L.; Love, J. B. *Chem. Eur. J.* **2013**, *19*, 10287.
(14) Arnold, P. L.; Pécharman, A.-F.; Lord, R. M.; Jones, G. M.; Hollis, E.; Nichol, G. S.; Maron, L.; Fang, J.; Davin, T.; Love, J. B. *Inorg. Chem.* **2015**, *54*, 3702.
(15) Arnold, P. L.; Hollis, E.; Nichol, G. S.; Love, J. B.; Griveau, J.-C.; Caciuffo, R.; Magnani, N.; Maron, L.; Castro, L.; Yahia, A.; Odoh, S. O.; Schreckenbach, G. *J. Am. Chem. Soc.* **2013**, *135*, 3841.
(16) Arnold, P. L.; Hollis, E.; White, F. J.; Magnani, N.; Caciuffo, R.; Love, J. B. *Angew. Chem. Int. Ed.* **2011**, *50*, 887.
(17) Odoh, S. O.; Schreckenbach, G. *Inorg. Chem.* **2013**, *52*, 245.
(18) Yahia, A.; Arnold, P. L.; Love, J. B.; Maron, L. *Chem. Commun.* **2009**, 2402.
(19) Hayton, T. W.; Wu, G. *Inorg. Chem.* **2009**, *48*, 3065.
(20) Schnaars, D. D.; Wu, G.; Hayton, T. W. *Inorg. Chem.* **2011**, *50*, 4695.
(21) Schnaars, D. D.; Wu, G.; Hayton, T. W. *J. Am. Chem. Soc.* **2009**, *131*, 17532.
(22) Pankhurst, J. R.; Bell, N. L.; Zegke, M.; Platts, L. N.; Lamfsus, C. A.; Maron, L.; Natrajan, L. S.; Sproules, S.; Arnold, P. L.; Love, J. B. *Chem. Sci.* **2017**, *8*, 108.
(23) Hayton, T. W.; Wu, G. *J. Am. Chem. Soc.* **2008**, *130*, 2005.
(24) Morris, D. E. *Inorg. Chem.* **2002**, *41*, 3542.
(25) Seong-Yun, K.; Hiroshi, T.; Yasuhisa, I. *J. Nucl. Sci. Technol.* **2002**, *39*, 160.
(26) Asadi, Z.; Shorkaei, M. R. *Spectrochim. Acta, Part A* **2013**, *105*, 344.
(27) Arnold, P. L.; Blake, A. J.; Wilson, C.; Love, J. B. *Inorg. Chem.* **2004**, *43*, 8206.
(28) Tamasi, A. L.; Barnes, C. L.; Walensky, J. R. *Radiochim. Acta.* **2013**, *101*, 631.
(29) Back, D. F.; Manzoni de Oliveira, G.; Schulz Lang, E.; Vargas, J. P. *Polyhedron* **2008**, *27*, 2551.
(30) Sarsfield, M. J.; Steele, H.; Helliwell, M.; Teat, S. J. *Dalton Trans.* **2003**, 3443.
(31) Berthet, J.-C.; Siffredi, G.; Thuery, P.; Ephritikhine, M. *Dalton Trans.* **2009**, 3478.
(32) Le Caër, S. *Water* **2011**, *3*, 235.
(33) Bouniol, P.; Bjergbakke, E. *J. Nucl. Mater.* **2008**, *372*, 1.
(34) Neculai, A.-M.; Cummins, C. C.; Neculai, D.; Roesky, H. W.; Bunkòczi, G.; Walfort, B.; Stalke, D. *Inorg. Chem.* **2003**, *42*, 8803.
(35) Neculai, D.; Roesky, H. W.; Neculai, A. M.; Magull, J.; Walfort, B.; Stalke, D. *Angew. Chem. Int. Ed.* **2002**, *41*, 4294.

Graphical Abstract